ELSEVIER

Earth and Planetary Science Letters 124 (1994) 171–184

EPSL

^{10}Be records of sediment cores from high northern latitudes: Implications for environmental and climatic changes

A. Eisenhauer [a], R.F. Spielhagen [b], M. Frank [a], G. Hentzschel [a], A. Mangini [a], P.W. Kubik [c], B. Dittrich-Hannen [c], T. Billen [a]

[a] *Heidelberger Akademie der Wissenschaften, Im Neuenheimer Feld 366, 69120 Heidelberg, Germany*
[b] *GEOMAR, Forschungszentrum für marine Geowissenschaften, Wischhofstrasse 1–3, 24148 Kiel, Germany*
[c] *Institut für Teilchenphysik, Eidgenössische Technische Hochschule, ETH-Hönggerberg, CH-8093 Zürich, Switzerland*

(Received June 15, 1993; revision accepted March 31, 1994)

Abstract

The ^{10}Be records of four sediment cores forming a transect from the Norwegian Sea at 70°N (core 23059) via the Fram Strait (core 23235) to the Arctic Ocean at 86°N (cores 1533 and 1524) were measured at a high depth resolution. Although the material in all the cores was controlled by different sedimentological regimes, the ^{10}Be records of these cores were superimposed by glacial/interglacial changes in the sedimentary environment. Core sections with high ^{10}Be concentrations ($> 1 \cdot 10^9$ at/g) are related to interglacial stages and core sections with low ^{10}Be concentrations ($< 0.5 \cdot 10^9$ at/g) are related to glacial stages. Climatic transitions (e.g., Termination II, 5/6) are marked by drastic changes in the ^{10}Be concentrations of up to one order of magnitude. The average ^{10}Be concentrations for each climatic stage show an inverse relationship to their corresponding sedimentation rates, indicating that the ^{10}Be records are the result of dilution with more or less terrigenous ice-rafted material. However, there are strong changes in the ^{10}Be fluxes (e.g., Termination II) into the sediments which may also account for the observed oscillations. Most likely, both processes affected the ^{10}Be records equally, amplifying the contrast between lower (glacials) and higher (interglacials) ^{10}Be concentrations. The sharp contrast of high and low ^{10}Be concentrations at climatic stage boundaries are an independent proxy for climatic and sedimentary change in the Nordic Seas and can be applied for stratigraphic dating (^{10}Be stratigraphy) of sediment cores from the northern North Atlantic and the Arctic Ocean.

1. Introduction

^{10}Be profiles measured in the water column of the open ocean show a nutrient-type behaviour, indicating that ^{10}Be is rapidly scavenged by sinking particles and removed from the uppermost layers of the ocean [2]. Thus, the flux of ^{10}Be in the water column depends on the intensity of particle flux and the biological activity in the euphotic zone, where large spatial variations in today's world ocean are observed [1,2]. The ^{10}Be flux from the water column into the marine sediments is relatively low in non-upwelling open-ocean areas [c.f. 1]. In contrast, ^{10}Be fluxes can be one order of magnitude higher in regions with enhanced supply of eroded terrigeneous material

[UC]

SSDI 0012-821X(94)00069-B

or with high biological productivity [c.f. 3–6]. This is attributed to the high affinity of ^{10}Be to clay minerals, which scavenge ^{10}Be very efficiently from the water column [7,8]. These small particles are those most likely to be adsorbed to larger particles of biogenic origin which rapidly trans-

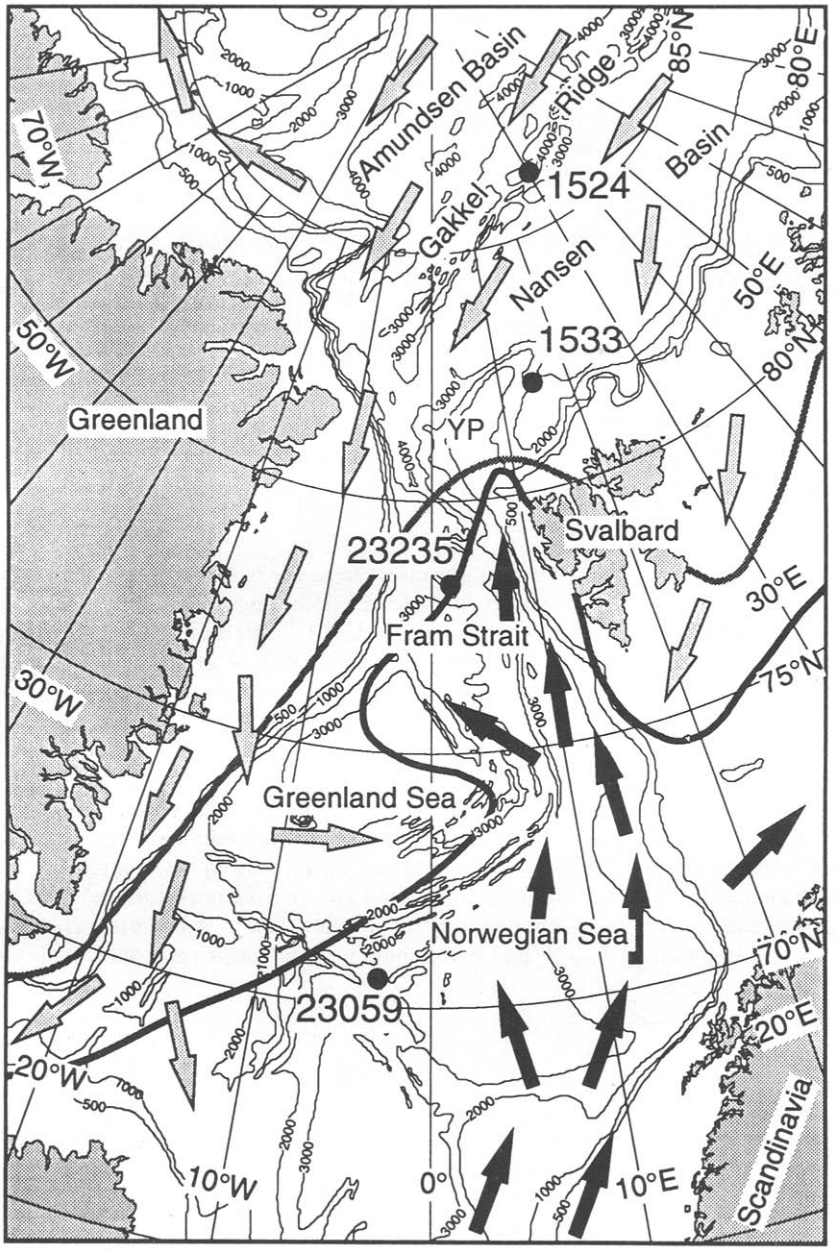

Fig. 1. Bathymetry of the Nordic Seas and the Arctic Ocean. The analysed cores are located along a transect from the Norwegian Sea (core 23059, ~ 70°N) via the Fram Strait (core 23235, ~ 78°N) and the Yermak Plateau (core 1533, ~ 82°N) to the eastern Arctic Ocean (core 1524, ~ 86°N). Darker arrows represent warm surface waters. Lighter arrows represent cold waters of the Beaufort Gyre (western Arctic Ocean), the Transpolar Drift (eastern Arctic Ocean) and the East Greenland Current.

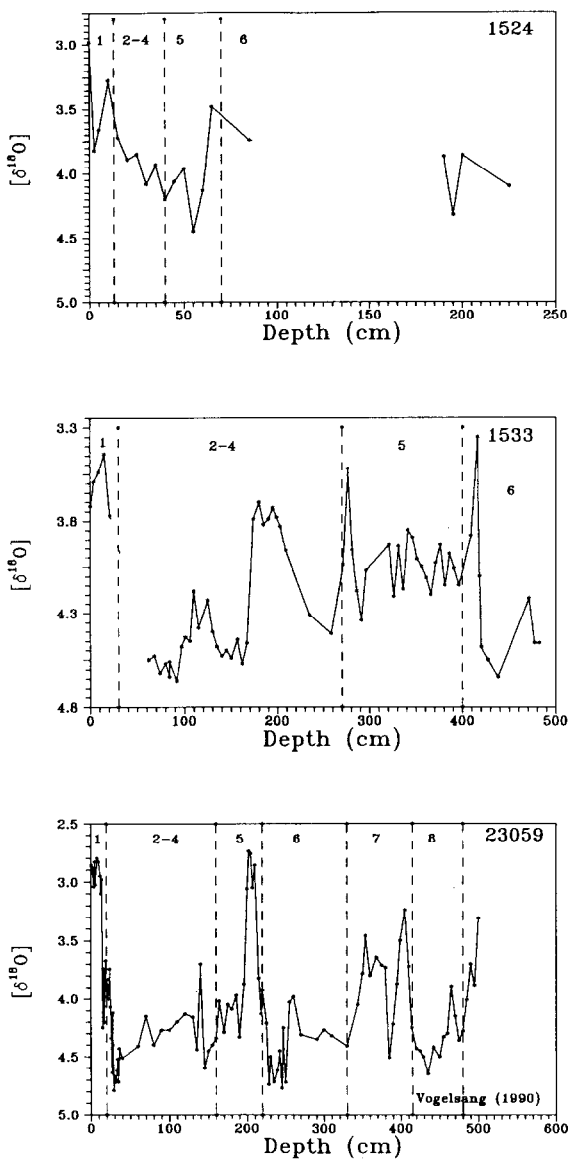

Fig. 2. In this figure the $\delta^{18}O$ (‰ vs. PDB) values are presented as a function of depth for cores 1524, 1533 and 23059. Vertical dotted lines divide the major climatic stages expressed as oxygen isotope stage boundaries [19,20]. Core 23059 can unambigously be correlated to the standard $\delta^{18}O$ curve and thus provides a reliable chronology. However, the $\delta^{18}O$ curves of the Arctic cores (1524, 1533) are not easy to interpret because there are core sections which are barren of planktic foraminifers and, in addition, these curves are influenced by isotopically light meltwater. Therefore, the position of the stages, as marked in this figure, is also based on additional chronological data (Fig. 3).

Table 1
Core locations and water depths

Core	Location	Water depth (m)
23059	70°18.3′N, 4°1.3′W	2281
23235	78°51.55′N, 1°18.59′E	2456
1533	82°1.9′N, 15°10.7′E	2030
1524	85°21.8′N, 26°12.9′E	3646

port ^{10}Be to the marine sediments [2]. However, biological productivity and the supply of such fine-grained material (e.g., clay) have not been constant throughout time, and have been controlled by changes in distinct environmental conditions and in the climate of the past. In particular, most drastic climatic and environmental changes occurred in the northern North Atlantic and Arctic Ocean.

In previous publications [6,9,17] it was reported that changes in the climatic and sedimentary environment are reflected by oscillations of the ^{10}Be and $^{230}Th_{ex}$ content in the sediments of the Nordic Seas. In the high-resolution record of core 23235 (Arctic Ocean, Fram Strait), climatic transitions are marked by drastic variations in the ^{10}Be and $^{230}Th_{ex}$ concentrations of up to one order of magnitude [6]. The observed changes in the ^{10}Be concentrations during times of rapid climatic transitions in this core indicate that climatic changes are instantaneously accompanied by changes in the environmental conditions (e.g., sedimentation rates, grain-size distribution, etc.) which either support or restrict the input of ^{10}Be into the sediments.

In the presently ice-covered areas of the northern North Atlantic and the Arctic Ocean, sedimentation is controlled by ice-rafting of terrigenous sediments [c.f. 9,10]. The amount of coarse-grained terrigenous material (> 63 μm) in sea-ice sediments of the Arctic Ocean is low compared to the dominating clay and silt grain sizes [10]. In the Nordic Seas climatic and environmental changes in the Late Quaternary are reflected by highly variable grain-size distributions and carbonate contents in the sediments [c.f. 11,12,13]. During glacial stages, the transport of coarse-grained, iceberg-rafted terrigenous material was enhanced, whereas in interglacial sediments the

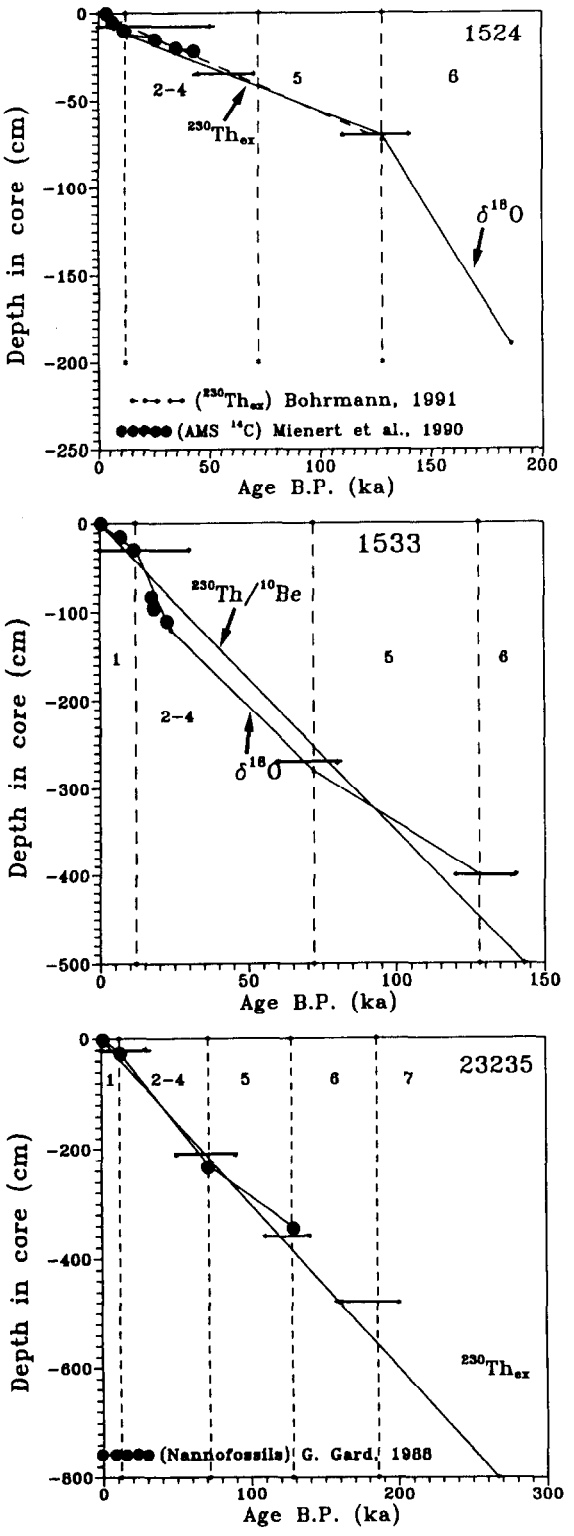

amount of coarse-grained material was significantly lower [11,13,14]. The high carbonate content (up to 15%) resulting from increased amounts of planktonic foraminifers and coccoliths in some of the interglacial Arctic sediments was most likely caused by a higher biological productivity in the Arctic Ocean [15,16]. During glacials a closed sea-ice cover restricted biological productivity in the northern North Atlantic and the Arctic Ocean [15,16].

For this study, high-resolution ^{10}Be records are presented from four high-latitude sediment cores (Table 1) along a transect from the Norwegian Sea (70°N) via the Fram Strait (78°N) to the Arctic Ocean (86°N) (Fig. 1). The chemical preparation of our ^{10}Be samples follows closely previously described procedures [18]. The ^{10}Be data are calibrated relative to an internal standard (S555, $^{10}Be/^{9}Be = 101.4 \cdot 10^{-12}$) at the Zürich AMS facility.

2. Core chronologies

Core 23059 from the Norwegian Sea is the only one that shows a $\delta^{18}O$ record (Fig. 2) which can be unambiguously correlated to the standard stable oxygen isotope curve [19,20]. In contrast to the Norwegian Sea, oxygen isotope records from the Arctic Ocean (Fig. 2) are either not available (23235) due to the low abundance of foraminifers in Arctic sediments or they are influenced by the input of isotopically light meltwater. Thus, the stable oxygen isotope records of these cores (1524, 1533) are not easy to interpret and additional chronological information (biostratigraphy, $^{230}Th_{ex}$ and AMS ^{14}C) must be taken into account to establish precise core chronologies. All the available chronological data are summarised in Fig. 3 and are discussed in detail below. The

Fig. 3. In these figures all available chronological data are summarised. Vertical broken lines mark oxygen isotope stage boundaries. Dots represent AMS ^{14}C datings of foraminifera in core 1524 and 1533 and biostratigraphic data in core 23235. Short horizontal lines represent drastic changes in the ^{10}Be concentrations. Within the uncertainties all the dating techniques applied to our cores are in good agreement.

Table 2
Average sedimentation rates and ^{10}Be concentrations

	1 (0–12 ka)	2–4 (12–72 ka)	5 (72–128 ka)	6 (128–186 ka)	Average
23059	1.7 (0.8)	2.2 (0.53)	1.3 (1.02)	1.9 (0.3)	~ 1.8 (0.62)
23235	1.7 (0.5)	3.2 (0.25)	2.6 (1.14)	2.1 (0.19)	~ 2.6 (0.52)
1533	2.3 (1.0)	4.3 (0.52)	2.0 (1.19)	–	~ 3.1 (0.86)
1524	1.2 (1.0)	0.35 (0.8)	0.6 (1.1)	1.9 (0.1)	~ 0.96 (0.68)

Average sedimentation rates (cm/ka = cm/1000 yr) are calculated from the depth range and the duration of the corresponding isotopic stages (Tables A1–A4). Average ^{10}Be concentrations (10^9 at/g) are calculated from Tables A1–A4 and are given in parentheses.

depths of the identified oxygen isotope stage boundaries and corresponding sedimentation rates are given in Tables A1-A4 and 2.

Core 1524: The δ^{18}O record (Fig. 2) of core 1524 reveals a poor depth resolution and several gaps in the core sections barren of planktic foraminifers. The position of oxygen isotope stage boundary 1/2 can be identified by interpolation of the available AMS ^{14}C data [24], which show that the last climatic transition corresponds to a core depth of about 13 cm. From the radioactive decay of the ^{230}Th$_{ex}$ data [14], an average sedi-

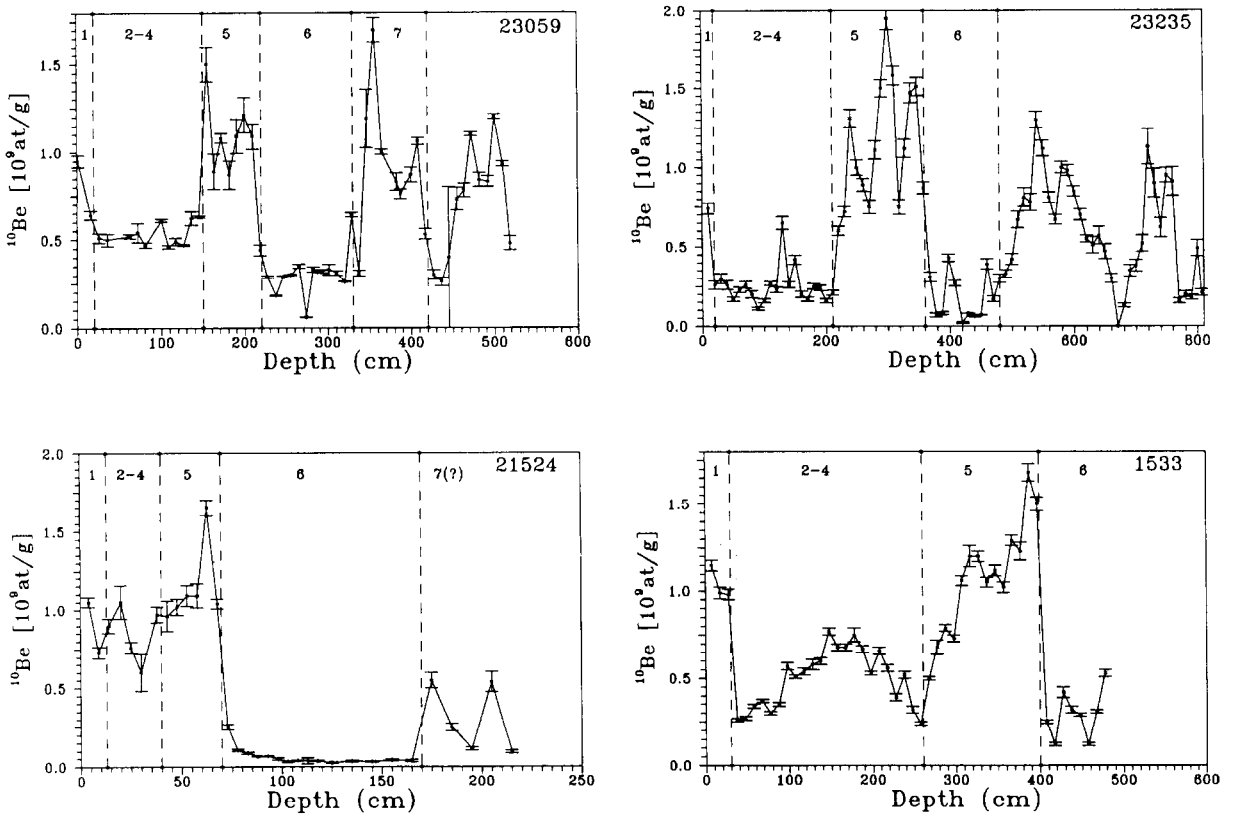

Fig. 4. The ^{10}Be records of the analysed cores are plotted versus depth in core. Vertical broken lines mark oxygen isotope stage boundaries. Note that interglacial stages (1, 5, 7) are characterised by high ^{10}Be concentrations whereas glacial stages (2–4, 6) are characterised by low ^{10}Be concentrations. Core sections corresponding to glacial/interglacial transitions are marked by drastic changes in the ^{10}Be concentrations (e.g., 4/5, 5/6, 6/7).

mentation rate of about 0.5 cm/ka can be calculated. This allows the identification of climatic transition 4/5 at 40 cm and that of 5/6 at 70 cm.

Core 1533: The $\delta^{18}O$ record of this core (Fig. 2) is most likely influenced by isotopically light meltwater and, like core 1524, reveals several gaps in core sections barren of planktic foraminifers. However, for verification of the major climatic transition $^{230}Th_{ex}$ and AMS ^{14}C data are available (Fig. 3). The climatic transition of stages 1/2 can be identified at about 30 cm by interpolation of the AMS ^{14}C data [22] (Fig. 3). From $^{230}Th_{ex}$ dating, a mean sedimentation rate of about 3.5 ± 0.4 cm/ka can be calculated for this core. Given this value the stage 4/5 boundary is expected at a depth of about 250 ± 30 cm, which is in accordance with the interpretations of the stable oxygen isotope record (Fig. 2). In this core, the 5/6 transition is apparently indicated by an isotopically light $\delta^{18}O$ peak at 420 cm. However, glacial/interglacial changes in Arctic sediments are in general characterised by a drastic change in the sediment composition from coarse- to fine-grained material, as has occurred in this core at about 400 cm (see Table A3). Therefore, we argue that the correct position of the 5/6 transition is at 400 cm, as indicated in Fig. 2 and 3. Thus, the peak at 420 cm is interpreted to reflect a meltwater excursion late in oxygen isotope stage 6.

Core 23235: For core 23235, no $\delta^{18}O$ stratigraphy is available due to negligible amounts of foraminifers. The chronology of this core is based on previously published $^{230}Th_{ex}$ [6] and biostratigraphic data [15], which are in good agreement with the positions of stage boundaries 1/2, 4/5 and 5/6. As an independent verification based on sedimentological and paleomagnetic parameters this core can be correlated to the neighbouring core 1535 (for which a complete $\delta^{18}O$ record exists). This comparison clearly confirms the positions of the stage boundaries as indicated in Fig. 2 and 3 [13,25].

Core 23059: The $\delta^{18}O$ stratigraphy of core 23059 from the Norwegian Sea was taken from Vogelsang [21]. In this core, the last four major climatic transitions can be unambiguously identified from the $\delta^{18}O$ record (Fig. 2).

3. ^{10}Be records

Results of the ^{10}Be measurements are listed in Tables A1–A4 and are displayed graphically in Fig. 4. Statistical errors are one standard deviation from the mean and are typically about 5% of the measured value. In addition, average ^{10}Be concentrations for each oxygen isotope stage are summarised in Table 2 together with the corresponding sedimentation rates. All the analysed cores show strong oscillations in their ^{10}Be records. The concentrations vary from less than $0.1 \cdot 10^9$ up to $2 \cdot 10^9$ at/g. In general, high ^{10}Be concentrations (average = ca. $1 \cdot 10^9$ at/g) are found in interglacial sediments (stages 1, 5, and 7), whereas low ^{10}Be concentrations (average = ca. $0.5 \cdot 10^9$ at/g) are measured in sediments of glacial stages 2–4 and 6. The stage boundaries, which represent rapid climatic transitions (e.g., 4/5, 5/6 and 6/7) are marked by drastic changes in the ^{10}Be concentrations of up to one order of magnitude (Table 2 and Fig. 3). Note that for verification of the 6/7 stage boundary no chronological data are available. These observations clearly show that climatic change during the Late Quaternary caused strong glacial/interglacial differences in the ^{10}Be deposition in the Nordic Seas.

4. Average sedimentation rates and ^{10}Be concentrations

The sedimentation rates of the cores (Table 2) vary between 0.5 cm/ka (core 1524, stages 2–5) and about 3.3 cm/ka (core 23235, stages 2–4). To eliminate regional variations and to extract the influence of climatic change onto sedimentation rates and ^{10}Be concentrations, these were normalised to their average core values. In Fig. 5 the normalised ^{10}Be concentrations are plotted as a function of the normalised sedimentation rates. This figure clearly shows that there is an inverse relationship between ^{10}Be concentrations and sedimentation rates. In addition, it can be seen that core sections related to glacial stages are characterised by high sedimentation rates and low ^{10}Be concentrations, whereas interglacial core

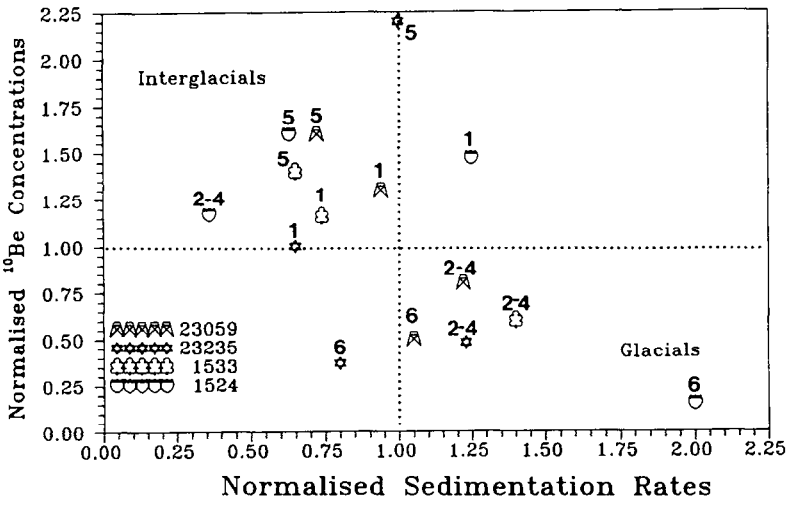

Fig. 5. Normalised ^{10}Be concentrations are plotted as a function of the corresponding normalised sedimentation rates for each climatic stage. Horizontal and vertical dotted lines mark average ^{10}Be concentrations and average sedimentation rates respectively. Labels above the data points refer to the isotope stages. Note that there is an inverse relationship between the ^{10}Be concentrations and the sedimentation rates. Glacial stages are characterised by increased sedimentation rates and lower ^{10}Be concentrations whereas during interglacial stages the reverse is seen.

sections are marked by low sedimentation rates and high ^{10}Be concentrations.

5. Grain-size records

Grain-size records (clay and coarse-grained fraction > 63 μm) are available for all cores (Tables A1–A4). Average glacial/interglacial values are calculated and summarised in Table 3. We note that the comparison of these records to our ^{10}Be profiles is difficult because the grain-size records were not measured at the same depth resolution. Furthermore, ^{10}Be concentrations and grain-size distribution were not determined on aliquot samples.

From Table 3 it can be seen that the clay concentrations in our Arctic cores (1533, 23235, 1524) vary between 20 and 67%. The relative abundance of the coarse-grained material (given in parentheses) in the Arctic cores usually amounts to $< 10\%$ during isotope stages 1–5. However, in the Arctic core sections, which represent stage 6, the abundance is by a factor of 2 higher than in the core section above. The calculation of correlation coefficients from the data given in Tables A1–A3 reveals only a slightly positive trend for clay and ^{10}Be and a weak inverse relationship between the coarse-grained material and ^{10}Be.

In contrast, the clay content of core 23059 from the Norwegian Sea tends to be lower and

Table 3
Grain-size distribution

	1 (0–12 ka)	2–4 (12–72 ka)	5 (72–128 ka)	6 (128–186 ka)	Average
23059	19 (11)	41 (14)	33 (22)	40 (16)	37 (17)
23235	20 (8)	44 (9)	67 (9)	57 (24)	53 (14)
1533	– (4)	– (4)	– (1)	– (14)	– (6)
1524	58 (6)	62 (3)	57 (8)	38 (20)	53 (10)

Average concentrations (%) of clay and coarse sediment fraction (> 63 μm, given in parentheses) are given for every isotopic stage in our cores.

Table 4
Average ^{10}Be fluxes

	1 (0.12 ka)	2–4 (12–72 ka)	5 (72–128 ka)	6 (128–186 ka)	Average
23059	1.2	1.1	1.3	0.6	1.0
23235	1.1	0.7	2.3	0.4	1.1
1533	2.0	2.0	2.0	–	2.0
1524	0.8	0.2	0.5	0.2	0.3

Average ^{10}Be fluxes ($10^9 \cdot$ at/cm$^2 \cdot$ ka) are presented for every isotopic stage. ^{10}Be fluxes are calculated from $F = C \cdot S \cdot D$, where F is the average ^{10}Be flux, C is the average ^{10}Be concentration, S is the average sedimentation rate and D is the average bulk density. Dry bulk densities are taken from Tables A1–A4. For core 1533, where no bulk density data are available, a mean bulk density of about 0.85 g/cm^3 is assumed.

the coarse-grained fraction content tends to be higher than in the Arctic cores. The clay concentrations are slightly higher during glacial stages, whereas the coarse-grained fraction is more abundant during the interglacial stages. This is also reflected by an inverse relationship between clay and ^{10}Be and a positive correlation between coarse-grained material and ^{10}Be.

We note that the clay records (Tables A1–A4) show a high-frequency change (e.g., 23059, 23235) in concentrations and, thus, do not show a significant relationship with the climatic evolution of the Late Quaternary. The abundance of coarse-grained material tends to be higher during glacial stages, although the occurrence of the coarse grained material (Tables A1–A4) in core sections related to glacial stages is patchy (1533), or shows a high-frequency fluctuation between high and low concentrations. Thus, in contrast to the ^{10}Be records, neither the records of the coarse-grained material nor the clay concentrations allow the identification of glacial/interglacial transitions.

Furthermore, it is noteworthy that although the grain-size distribution reveals that the sedimentological conditions were different in the Arctic Ocean and the Norwegian Sea, all cores show similar patterns in their ^{10}Be records. This indicates that local variations in the sediment composition were of minor importance for the ^{10}Be records compared to the influence of the sedimentation rates.

6. ^{10}Be fluxes

Average ^{10}Be fluxes for every climatic stage were calculated from the average ^{10}Be concentrations (Table 2), the average dry bulk densities (Tables A1–A4), and the average sedimentation rates (Table 2). The results of the ^{10}Be flux calculations are summarised in Table 4. It can be seen that the ^{10}Be fluxes vary between a minimum flux of ca. 0.2×10^9 at/cm$^2 \cdot$ ka and a maximum flux of ca. 2.3×10^9 at/cm$^2 \cdot$ ka. The minimum value is lower by a factor of ~ 6 and the maximum value is higher by a factor of 2 than the expected value for the present-day average ^{10}Be production in the atmosphere ($\sim 1.2 \times 10^9$ at/cm$^2 \cdot$ ka, [23]). To eliminate the influence of local sedimentological conditions, the calculated fluxes were normalised to their average core value (Fig. 6). This figure shows that the normalised ^{10}Be fluxes are related to the climatic evolution of the Late Quaternary. With the exception of core 1533, all cores indicate that the ^{10}Be input was enhanced during interglacial stages, whereas fluxes are lower than average during glacial stages. In particular, the ^{10}Be fluxes of stages 5 and 6 are markedly different.

7. Discussion

The pattern of the ^{10}Be concentrations is similar in all cores, even though the sediments were controlled by different sedimentological and environmental regimes during the Late Quaternary (as seen from the grain-size records). This indicates that the local conditions influencing ^{10}Be deposition are superimposed by general changes in the sedimentary environment controlling the ^{10}Be deposition in the Nordic Seas. There are two key observations which account for the observed phenomena: (1) the inverse relationship

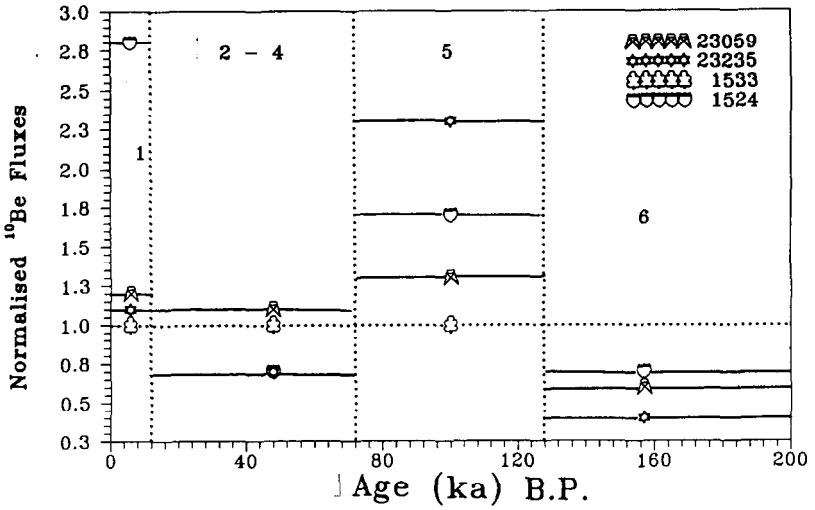

Fig. 6. In this figure the normalised ^{10}Be fluxes are plotted as a function of their corresponding age (B.P., ka = 1000 yr). Vertical dotted lines mark isotopic stage boundaries. The horizontal dotted line marks the core average of the ^{10}Be fluxes. It can be seen that the normalised ^{10}Be fluxes tend to be higher during interglacial stages and lower during glacial stages. In particular, the average ^{10}Be fluxes during stage 5 and 6 are markedly different.

between sedimentation rate and the ^{10}Be concentrations (Fig. 5) and (2) the glacial/interglacial variations in the ^{10}Be fluxes into the sediments (Fig. 6). Observation (1) indicates that the ^{10}Be oscillations are caused by variable dilution with terrigenous material, whereas observation (2) indicates that, in addition, these oscillations were also caused by variations in the ^{10}Be fluxes into the Nordic Seas. It is noteworthy that both processes (dilution and flux variations) affect the ^{10}Be records equally, amplifying the strong contrast between lower (glacials) and higher (interglacials) ^{10}Be concentrations. To understand these observations, we discuss simple qualitative models of the glacial/interglacial change in the sedimentary environment of the Nordic Seas. First we focus our attention on observation (1) and then we discuss observation (2).

In our model, we assume that during glacial periods the Arctic Ocean and the northern North Atlantic were covered with permanent sea ice extending south of 70°N. Icebergs were delivered to the open Arctic Ocean from the glaciated circum-Arctic continents. Sea ice and icebergs were transported together with the Arctic Transpolar Drift (Fig. 1) towards the Fram Strait where they entered the northern North Atlantic. Sea ice predominantly carried fine-grained sediment, which is incorporated in shallow waters by suspension freezing [26], whereas icebergs carried large amounts of eroded coarse-grained material [27]. During transport, parts of the sediment load were released from the ice and contributed significantly to the sedimentation in the glacial Arctic Ocean. While sinking through the water column, dissolved elements such as Be were scavenged, mainly by clay particles. At glacial/interglacial transitions environmental conditions changed. The permanent sea ice border shifted northward and the occurrence of icebergs was significantly reduced due to the wasting of the glacial ice caps. During interglacials the ice cover in the Arctic Ocean was dominated by sea ice and the input of eroded coarse terrigenous material was significantly reduced.

These environmental scenarios predict high sedimentation rates during glacials due to enhanced continental erosion but lower rates during interglacials. In addition, relatively high ^{10}Be concentrations are predicted for interglacial sediments and lower ^{10}Be concentrations are predicted for glacial sediments, under the assumption that the ^{10}Be flux remained constant at glacial/interglacial transitions. These predictions

are in accordance with our observations (Figs. 4 and 5). Thus, concerning observation (1) our data indicate that the variations in the ^{10}Be concentrations are influenced by the climatically controlled variations in the amount of eroded material. The influence of local and temporal variations in the particle grain size seems to be less important in these cores. However, during stage 6, the relatively high abundance of coarse-grained material may have additionally amplified the dilution effect, increasing the glacial/interglacial contrast between high and low ^{10}Be concentrations.

The glacial/interglacial variations in the ^{10}Be concentrations may also be explained by oscillations in the strength of the various ^{10}Be sources, as indicated by observation (2). Independent of the climatic influence there are two major sources of ^{10}Be in the Arctic Ocean. These are ^{10}Be which was already fixed onto ice-rafted sediments (source A) and ^{10}Be which was scavenged by particles while sinking through the water column (source B). Up to now only two ^{10}Be measurements of ice-rafted material (source A, clay sampled on Arctic sea ice floes at about 77°N) exist, yielding ^{10}Be concentrations of $0.22(\pm 0.01) \cdot 10^9$ at/g and $0.28(\pm 0.01) \cdot 10^9$ at/g. These concentrations are equal to or even lower than those measured in core sections corresponding to glacial stages. These measurements indicate that the variations in the strength of source (A) have only a minor influence on the ^{10}Be concentrations of the sediments. Thus, the major part of the glacial/interglacial oscillations of the ^{10}Be fluxes in our cores must be ascribed to variations in the ^{10}Be concentrations in the water column of the Arctic Ocean. During glacial stages in particular, the ^{10}Be concentration of the water column of the Arctic Ocean must have been significantly lower. Permafrost and continental ice sheets inhibited the input of Siberian river waters. Pacific waters could not enter the Arctic Ocean through the Bering Strait and the influx of Atlantic waters was strongly reduced [16,21]. In addition, the coverage of the Nordic Seas with sea ice and its drift to the northern North Atlantic inhibited the atmospheric deposition of ^{10}Be onto the sea surface. Hence, in the glacial Arctic Ocean only lower amounts of ^{10}Be atoms could be scavenged by particles while sinking through the water column. At glacial/interglacial transitions environmental conditions changed, allowing higher ^{10}Be concentrations in the water column and, hence, higher ^{10}Be fluxes into the sediments.

Due to insufficient data we cannot yet quantify the glacial/interglacial contribution of the sources to the total ^{10}Be flux into the Nordic Seas. However, our data reveal that the ^{10}Be concentration of the Arctic Ocean (source B) was probably significantly reduced during glacial stages (e.g., during stage 6) but enhanced during interglacial stages (e.g., 5), whereas the strength of source A remained more or less constant throughout time.

8. Summary

We argue that the observed pattern of high and low ^{10}Be concentrations in the sediments of the Nordic Seas is controlled by two processes: (1) dilution caused by glacial/interglacial changes in the sediment accumulation and (2) glacial/interglacial variation in the input of ^{10}Be into the Nordic Seas. Drastic changes in the ^{10}Be concentrations at glacial/interglacial transitions are time markers which can be applied for stratigraphic dating (^{10}Be stratigraphy) of key sediment cores from the Arctic Ocean and the northern North Atlantic.

Acknowledgements

Funding for this study was provided by the *Paläoklimaprojekt* of the Federal Republic of Germany. We thank H. Bohrmann, J. Scholten, H. Paetsch and R. Botz for providing material from cores 23059, 23235 and 1524 and for helpful discussion and comments. H. Erlenkeuser and the staff of the ^{14}C laboratory at Kiel University are acknowledged for performing the oxygen isotope measurements. We gratefully acknowledge J. Thiede and H. Kassens from the GEOMAR for their generous support and discussion. The critical comments of two anonymous reviewers helped significantly in improving the manuscript.

Appendix: Data

Table A1
^{10}Be, coarse fraction, clay and bulk density of core 23059

Depth (cm)	Isotope stage	^{10}Be (10^9 at/g)	Coarse fraction (> 63 μm) (%)	Clay (%)	Bulk density (g/cm^3)
0– 2	1	0.95 ±0.03	1	7	
11– 21		0.64 ±0.02	21	31	0.87
21– 31		0.51 ±0.03	12	51	0.87
57– 67		0.52 ±0.04	12	43	0.97
67– 77		0.54 ±0.01	16	37	0.96
77– 85		0.47 ±0.01	10	48	0.99
95–105	2–4	0.61 ±0.01	17	38	0.99
105–112		0.46 ±0.01	15	39	0.99
112–122		0.49 ±0.02	16	39	0.99
122–132		0.474±0.004	14	36	1.03
132–140		0.62 ±0.04	12	44	1.00
140–150		0.633±0.006	20	36	1.00
150–160		1.5 ±0.1	23	30	1.04
160–167		0.89 ±0.1	25	30	1.02
167–177		1.08 ±0.03	16	31	0.96
177–187		0.87 ±0.08	23	38	0.97
187–195	5	1.09 ±0.09	21	32	0.99
195–205		1.21 ±0.1	32	24	0.96
205–215		1.09 ±0.07	19	37	0.85
215–222		0.44 ±0.03	15	44	1.02
222–232		0.291±0.007	27	28	1.07
232–242		0.18 ±0.002	9	30	1.15
242–250		0.295±0.007	13	42	0.9
250–260		0.308±0.003	9	54	1.1
260–270		0.35 ±0.01	13	36	1.03
270–277	6	0.062±0.001	30	22	1.00
277–287		0.33 ±0.01	11	50	1.2
287–297		0.32 ±0.01	12	48	0.97
297–305		0.33 ±0.03	14	41	0.95
305–315		0.31 ±0.01	20	40	1.09
315–325		0.26 ±0.003	18	39	1.22
325–332		0.64 ±0.01	12	50	1.25
332–342		0.31 ±0.02	17	33	1.08
342–352		1.2 ±0.2	24	35	0.97
352–360		1.76 ±0.07	24	36	0.98
360–370	7–	1.0 ±0.1	14	35	1.02
380–385		0.83 ±0.05	17	30	0.96
385–395		0.76 ±0.03	15	33	0.93
395–405		0.87 ±0.04	20	36	1.04
405–412		1.06 ±0.02	15	42	0.95
412–422		0.53 ±0.03	21	36	1.05
422–432		0.3 ±0.03	24	33	1.23
432–440		0.26 ±0.02	25	26	1.32
440–450		0.4 ±0.4	17	38	1.15
450–460		0.73 ±0.07	18	40	0.97
460–467		0.78 ±0.04			
467–477		1.1 ±0.1	22	36	1.08
477–487		0.84 ±0.04			
487–495		0.83 ±0.03	22	37	1.02
495–505		1.2 ±0.01	21	37	0.97
505–515		0.93 ±0.02	13	43	0.91
515–522		0.48 ±0.04	38	28	1.01

Note: All reported statistical errors are one standard deviations from the mean (at/g = atoms per grame of sample weight). Coarse fraction, clay and bulk density data are from [21]. Statistical errors of these measurements are about 5%. Horizontal lines mark depth of oxygen isotope stage boundaries. The calculation of correlation coefficients reveals that there is a positive correlation between the coarse fraction and ^{10}Be ($r = 0.25$) and an inverse correlation of clay with ^{10}Be ($r = -0.23$). However, the coefficients are statistically not significant.

Table A2
^{10}Be, coarse fraction, clay and bulk density of core 23235

Depth (cm)	Isotope stage	^{10}Be (10^9 at/g)	Coarse fraction (> 63 μm) (%)	Clay (%)	Bulk density (g/cm^3)
0– 10	1	0.74±0.03	8	20	0.46
10– 20		0.26±0.03			
20– 30		0.3 ±0.03			
30– 40		0.26±0.03	8	29	1.1
40– 50		0.17±0.01			
50– 60		0.23±0.02			
60– 70		0.26±0.02			
70– 80		0.2 ±0.02			
80– 90		0.11±0.01	14	49	0.76
90–100		0.16±0.01			
100–110		0.27±0.01			
110–120	2–4	0.23±0.02			
120–130		0.65±0.04	9	49	0.6
130–140		0.26±0.02			
140–150		0.42±0.03	7	45	0.82
150–160		0.2 ±0.02			
160–170		0.17±0.01			
170–180		0.25±0.02	5	46	0.8
180–190		0.24±0.02			
190–200		0.16±0.01			
200–210		0.21±0.02			
210–220		0.6 ±0.03	9	70	0.7
220–230		0.72±0.03			
230–240		1.31±0.05	14	61	0.9
240–250		1.00±0.05			
250–260		0.89±0.04	13	64	1.0

Table A2 (continued)

Depth (cm)	Isotope stage	^{10}Be (10^9 at/g)	Coarse fraction (> 63 μm) (%)	Clay (%)	Bulk density (g/cm^3)
260–270		0.75 ± 0.04			
270–280		1.11 ± 0.06			
280–290		1.5 ± 0.05			
290–300	5	1.95 ± 0.07	6	69	0.62
300–310		1.58 ± 0.06			
310–318		0.75 ± 0.05			
318–328		1.12 ± 0.06			
328–338		1.47 ± 0.06	3	68	0.71
338–348		1.51 ± 0.06			
348–358		0.87 ± 0.04			
358–368		0.31 ± 0.03			
368–378		0.07 ± 0.01	3	69	1.03
378–388		0.08 ± 0.01			
388–398		0.43 ± 0.02			
398–408		0.27 ± 0.02			
408–420		0.02 ± 0.006	35	43	0.84
420–430	6	0.08 ± 0.001			
430–440		0.06 ± 0.002	32	51	0.85
440–450		0.07 ± 0.002			
450–460		0.39 ± 0.03	24	63	0.85
460–470		0.17 ± 0.02			
470–480		0.3 ± 0.03			
480–490		0.33 ± 0.02			
490–500		0.42 ± 0.04	12	68	
500–510		0.67 ± 0.05			
510–520		0.81 ± 0.06			
520–530	7–	0.78 ± 0.06			
530–540		1.3 ± 0.05	13	33	
540–550		1.12 ± 0.05			
550–560		0.81 ± 0.03			
560–570		0.67 ± 0.03			
570–580		1.04 ± 0.04	3	41	
580–590		0.98 ± 0.03			
590–600		0.85 ± 0.03			
600–610		0.7 ± 0.03			
610–620		0.55 ± 0.02	13	37	
620–630		0.51 ± 0.05			
630–640		0.57 ± 0.06	2	46	
640–650		0.47 ± 0.05			
650–660		0.34 ± 0.03	33	18	
660–670					
670–680		0.13 ± 0.01			
680–690		0.35 ± 0.04			
690–700		0.38 ± 0.04	12	44	
700–710		0.52 ± 0.05			
710–720		1.13 ± 0.13			
720–730		0.94 ± 0.09			
730–740		0.62 ± 0.06	12	41	
740–750		0.95 ± 0.05			
750–760		0.91 ± 0.1			
760–770		0.16 ± 0.02			

Table A2 (continued)

Depth (cm)	Isotope stage	^{10}Be (10^9 at/g)	Coarse fraction (> 63 μm) (%)	Clay (%)	Bulk density (g/cm^3)
770–780		0.22 ± 0.02			
780–790		0.18 + 0.02			
790–800		0.49 ± 0.05	11	37	
800–806		0.21 ± 0.02			

All reported statistical errors are one standard deviation from the mean (at/g = atoms per gramme sample weight). Coarse fraction, clay and bulk density data are from Botz [pers. commun., 1993]. Heavy horizontal lines mark depth of oxygen isotope stage boundaries. The calculation of the correlation coefficients shows that there is a positive correlation between ^{10}Be and clay ($r = 0.25$) and an inverse correlation between ^{10}Be and the coarse fraction ($r = -0.34$). However, the correlation coefficients are statistically not significant.

Table A3
^{10}Be, ^{230}Th$_{ex}$ and coarse fraction of core 1533

Depth (cm)	Isotope stage	^{10}Be (10^9 at/g)	^{230}Th$_{ex}$ (dpm/g)	Coarse fraction (> 63 μm) (%)
0 – 7.5		1.15 ± 0.03	5.06 ± 0.3	4.7
7.5 – 17.5	1	0.99 ± 0.03	4.63 ± 0.3	4.6
17.5–27.5		0.98 ± 0.03	4.33 ± 0.3	2.9
27.5– 37.5		0.26 ± 0.01	1.84 ± 0.3	17.4
37.5– 47.5		0.27 ± 0.01	0.86 ± 0.3	3
47.5– 57.5		0.34 ± 0.01	1.09 ± 0.3	3
57.5– 67.5		0.37 ± 0.01	2.31 ± 0.3	3
67.5– 77.5		0.30 ± 0.01	1.35 + 0.3	22
77.5– 87.5		0.35 ± 0.01	1.28 ± 0.3	32
87.5– 97.5		0.57 ± 0.02	2.09 ± 0.3	
97.5–107.5		0.51 ± 0.01	2.02 ± 0.3	
107.5–117.5		0.54 ± 0.02	21.4 ± 0.3	
117.5–127.5		0.58 ± 0.03	1.61 ± 0.3	0.3
127.5–137.5		0.60 ± 0.02	1.81 ± 0.3	0.22
137.5–147.5		0.77 ± 0.02	2.2 ± 0.3	0.38
147.5–157.5		0.68 ± 0.02	1.77 ± 0.3	1.16
157.5–167.5		0.68 ± 0.02	2.11 ± 0.3	0.62
167.5–177.5		0.75 ± 0.04	2.50 ± 0.3	0.77
177.5–187.5		0.67 ± 0.02	2.04 ± 0.3	1.43
187.5–197.5		0.53 ± 0.01	2.18 ± 0.3	0.68
197.5–207.5	2–4	0.66 ± 0.02	3.31 ± 0.3	4.2
207.5–217.5		0.56 ± 0.02	1.69 ± 0.3	
217.5–227.5		0.39 ± 0.02	1.28 ± 0.3	3.52
227.5–237.5		0.52 ± 0.02	1.05 ± 0.3	6.85
237.5–247.5		0.32 ± 0.01	0.88 ± 0.3	0.15
247.5–257.5		0.24 ± 0.01	0.76 ± 0.3	0.08
257.5–267.5		0.50 ± 0.01	1.10 ± 0.3	0.45
267.5–277.5		0.68 ± 0.01	1.64 ± 0.3	0.37
277.5–287.5		0.79 ± 0.04	1.93 ± 0.3	0.08

Table A3 (continued)

Depth (cm)	Isotope stage	^{10}Be (10^9 at/g)	$^{230}Th_{ex}$ (dpm/g)	Coarse fraction (> 63 μm) (%)
287.5–297.5		0.73 ± 0.02	2.18 ± 0.3	4.2
297.5–307.5		1.06 ± 0.02	1.46 ± 0.3	0.55
307.5–317.5		1.20 ± 0.03	1.84 ± 0.3	0.28
317.5–327.5		1.20 ± 0.06	1.98 ± 0.3	0.21
327.5–337.5		1.05 ± 0.03	2.04 ± 0.3	0.22
337.5–347.5	5	1.12 ± 0.03	2.60 ± 0.3	2
347.5–357.5		1.02 ± 0.03	2.32 ± 0.3	
357.5–367.5		1.29 ± 0.05	1.98 ± 0.3	1.62
367.5–377.5		1.23 ± 0.05	2.01 ± 0.3	2
377.5–387.5		1.68 ± 0.05	1.79 ± 0.3	0.64
387.5–397.5		1.50 ± 0.04	1.40 ± 0.3	0.32
397.5–407.5		0.25 ± 0.01	0.34 ± 0.3	23
407.5–417.5		0.12 ± 0.01	0.71 ± 0.3	19
417.5–427.5		0.42 ± 0.03	0.77 ± 0.3	7
427.5–437.5	6–	0.32 ± 0.02	0.27 ± 0.3	7
437.5–447.5		0.29 ± 0.01	0.48 ± 0.3	20
447.5–457.5		0.12 ± 0.01	0.03 ± 0.3	26
457.5–467.5		0.31 ± 0.01	0.58 ± 0.3	8
467.5–477.5		0.53 ± 0.02	1.25 ± 0.3	0.2

All reported statistical errors are one standard deviation from the mean (at/g = atoms per gramme of sample weight). Dpm/g = decays per minute per gramme of sample weight. From the $^{230}Th_{ex}$ record (normalized to ^{10}Be) a mean sedimentation rate of about 3.5 ± 0.4 cm/ka can be calculated. Heavy horizontal lines mark oxygen isotope stage boundaries.

Table A4
^{10}Be, coarse fraction, clay and bulk density of core 1524

Depth (cm)	Isotope stage	^{10}Be (10^9 at/g)	Coarse fraction (%)	Clay (%)	Bulk density (g/cm^3)
4		1.05 ± 0.03	3.5	57	0.6
9	1	0.73 ± 0.04	7.6	58	0.8
14		0.94 ± 0.04			
20		1.1 ± 0.1			
25	2–4	0.76 ± 0.04			
30		0.61 ± 0.1	3	62	0.7
38		0.97 ± 0.05			
43		0.96 ± 0.09			
48		1.02 ± 0.05	11	50	0.9
53	5	1.09 ± 0.06			
58		1.09 ± 0.08			
63		1.65 ± 0.05	4	63	0.7
68		1.04 ± 0.03			
73		0.25 ± 0.02	22	40	1.5
78		0.105 ± 0.0063			
83		0.086 ± 0.006	13	43	1.3
88		0.065 ± 0.005			
93		0.0667 ± 0.004			
98		0.048 ± 0.007			
105	6–	0.032 ± 0.005			
108		0.038 ± 0.004	23	35	1.4
113		0.04 ± 0.01			
118		0.036 ± 0.004			
125		0.025 ± 0.004			
135		0.034 ± 0.005	26	32	1.3
145		0.033 ± 0.005			
155		0.042 ± 0.006			
165		0.037 ± 0.007	25	30	1.4
175		0.55 ± 0.05			
185		0.25 ± 0.025	10	46	1.3
195		0.114 ± 0.009	9	56	1.0
205		0.54 ± 0.06	35	24	1.2
215		0.095 ± 0.009			

All reported statistical errors are one standard deviation from the mean (at/g = atoms per gramme of sample weight). Sand, clay and bulk density data are from [14]. Heavy horizontal lines mark oxygen isotope stage boundaries. The calculation of the correlation coefficients shows that there is a positive correlation between ^{10}Be and clay ($r = 0.62$) and an inverse correlation between ^{10}Be and the coarse fraction ($r = -0.55$).

References

[1] Y. Lao, R.F. Anderson, W.S. Broecker, S.E. Trumbore, H.J. Hofmann and W. Wölfli, Transport and burial rates of ^{10}Be and ^{231}Pa in the Pacific during the Holocene period, Earth Planet. Sci. Lett. 113, 173–189, 1992.

[2] M. Kusakabe, T.-L. Ku, J.R. Southon, J.S. Vogel, D.E. Nelson, C.I. Measures and Y. Nozaki, Distribution of ^{10}Be and ^{9}Be in the Pacific Ocean, Earth Planet. Sci. Lett. 82, 231–240, 1987.

[3] A. Mangini, M. Segl, G. Bonani, H.J. Hofmann, E. Morenzoni, M. Nessi, M. Suter, W. Wölfli and K.K. Turekian. Mass spectrometric ^{10}Be dating of deep-sea sediments applying the Zürich tandem accelerator, Nucl. Instrum. Meth. Phys. Res. B5, 353–358, 1984.

[4] L. Brown, J. Klein and R. Middleton. Anomalous isotopic concentrations in the sea off Southern California, Geochim. Cosmochim. Acta 49, 153–157, 1985.

[5] A. Eisenhauer, A. Mangini, M. Segl, J. Beer, G. Bonani, M. Suter and W. Wölfli. High resolution ^{10}Be and ^{230}Th profiles in DSDP Site 580, Nucl. Instrum. Meth. Phys. Res. B29, 326–331, 1987.

[6] A. Eisenhauer, A. Mangini, R. Botz, P. Walter, G. Bonani, M. Suter, H.J. Hofmann and W. Wölfli. High resolution ^{230}Th and ^{10}Be stratigraphy of late Quater-

nary sediments from the Fram Strait (core 23235), in: Geological History of the Polar Oceans: Arctic versus Antarctic, U. Bleil and J. Thiede, eds., pp. 475–487, Kluwer, 1990.

[7] J.R. Southon, T.-L. Ku, D.E. Nelson, J.L. Reyss, J.C. Duplessy and J.S. Vogel, ^{10}Be in a deep-sea core: implications regarding ^{10}Be production changes over the past 420 ka, Earth Planet Sci. Lett. 85, 356–364.

[8] P. Sharma, R. Mahannah, W.S. Moore, T.L. Ku and J.R. Southon. Transport of ^{10}Be and ^{9}Be in the ocean, Earth Planet. Sci. Lett. 86, 69–76, 1987.

[9] D. Hebbeln and G. Wefer, Effects of ice coverage and ice rafted material on sedimentation in the Fram Strait, Nature 350, 409–411, 1991.

[10] S. Pfirman, J.-C. Gascard, I. Wollenburg, P.J. Mudie and A. Abelmann, Particle-laden Eurasian Arctic sea ice: observations from July and August 1987, Polar Res. 7, 59–66, 1989.

[11] R. Henrich, H. Kassens, E. Vogelsang and J. Thiede, Sedimentary facies of glacial–interglacial cycles in the Norwegian Sea during the last 350 ka, Mar. Geol. 86, 283–319, 1989.

[12] J. Bischof, J. Koch, M. Kubisch, R. Spielhagen and J. Thiede, Nordic Sea surface ice drift reconstructions—evidence from ice-rafted coal fragments during oxygen isotope stage 6, in: Glacimarine Environments: Processes and Sediments, J.A. Dowdeswell and J.D. Scourse, eds., Geol. Soc. London Spec. Publ., 53, 275–291, 1990.

[13] S. Köhler and R.F. Spielhagen. The enigma of oxygen isotope stage 5 in the central Fram Strait, in: Geological History of the Polar Oceans: Arctic versus Antarctic, U. Bleil and J. Thiede, eds., pp. 489–497, Kluwer, 1990.

[14] H. Bohrmann. Radioisotope Stratigraphy, Sedimentology and Geochemistry of Late Quaternary Sediments from the Eastern Arctic Ocean (Reports on Polar Research), Alfred-Wegener-Inst., Bremerhaven, 1991.

[15] G. Gard, Late Quaternary calcareous nannofossil biozonation, chronology and paleo-oceanography in areas north of the Faeroe–Iceland Ridge, Quat. Sci. Rev. 2, 65–73, 1988.

[16] G. Gard and J. Backman, Synthesis of Arctic and sub-Arctic coccolith biochronology and history of North Atlantic Drift Water influx during the last 500,000 years, in: Geological History of the Polar Oceans: Arctic versus Antarctic, U. Bleil and J. Thiede, eds., pp. 417–436, Kluwer, 1990.

[17] J.C. Scholten, R. Botz, A. Mangini, H. Paetsch, P. Stoffers and E. Vogelsang, High resolution $^{230}Th_{ex}$ stratigraphy of sediments from high-latitude areas (Norwegian Sea, Fram Strait), Earth Planet. Sci. Lett. 101, 54–62, 1990.

[18] W.U. Henken-Mellies, J. Beer, F. Heller, K.J. Hsü, C. Shen, G. Bonani, H.J. Hofmann and W. Wölfli, ^{10}Be and ^{9}Be in South Atlantic DSDP Site 519: Relation to geomagnetic reversals and to sediment composition, Earth Planet. Sci. Lett. 98, 267–276, 1990.

[19] D.G. Martinson, N.G. Pisias, J.D. Hays, J. Imbrie, T.C. Moore and N.J. Shackelton, Age dating and the orbital theory of the ice ages: Development of a high resolution 0 to 300000 year chronostratigraphy, Quat. Res. 27, 1–29, 1987.

[20] J. Imbrie, J.D. Hays, D.G. Martinson, A. McIntyre, A.C. Mix, J.J. Morley, N.G. Pisias, W.L. Prell and N. Shackleton, The orbital theory of Pleistocene climate: Support from a revised chronology of the marine δ^{18}O record, in: Milankovitch and Climate 1, G. Kukla and B. Saltzmann, eds., pp. 269–305, Reidel, 1984.

[21] E. Vogelsang. Paläoozeanographie des Europäischen Nordmeeres anhand von stabilen C- und O-Isotopen, Ber. Sonderforschungsber. 313, 23, 136 pp., 1990.

[22] S.E.I. Köhler. Spätquatäre paläo-ozeanographische Entwicklung des Nordpolarmeeres anhand von Sauerstoff- und Kohlenstoffisotopenverhältnissen der planktischen Foraminifere *Neogloboquadrina Pachiderma* (sin.), GEOMAR Rep. 13, 103 pp., 1992.

[23] M.C. Monaghan, S. Krishnaswami and K.K. Turekian. The Global-average production rate of ^{10}Be, Earth Planet. Sci. Lett. 76, 279–287, 1985/1986.

[24] J. Mienert, L.A. Mayer, G.A. Jones and J.W. King, Physical and acoustic properties of Arctic ocean deep-sea sediments: Paleoclimatic implications, in: Geological History of the Polar Oceans: Arctic versus Antarctic, U. Bleil and J. Thiede, eds., pp. 475–487, Kluwer, 1990.

[25] N.R. Nowaczyk and M. Baumann, Combined high-resolution magnetostratigraphy and nannofossil biostratigraphy for late Quaternary Arctic Ocean seiments, Deep-Sea Res. 39 (Suppl. 2), 567–601, 1992.

[26] E.W. Kempema, E. Reimnitz and P.W. Barnes. Sea ice sediment entrainment and rafting in the Arctic, J. Sediment. Petrol. 59, 308–317, 1989.

[27] D.L. Clark and A. Hanson. Central Arctic Ocean sediment texture: a key to ice transport mechanism, in: Glacial–Marine Sedimentation, B.F. Molnia, ed., pp. 301–330, Plenum, 1983.